Int J Adv Manuf Technol (2012) 63:797–815
DOI 10.1007/s00170-012-3943-4

ORIGINAL ARTICLE

Experimental investigation of tool vibration and surface roughness in the precision end-milling process using the singular spectrum analysis

Chih-Cherng Chen · Nun-Ming Liu · Ko-Ta Chiang · Hua-Lun Chen

Received: 16 August 2011 / Accepted: 10 January 2012 / Published online: 28 February 2012

Abstract The vibrations on the cutting tool have a momentous influence for the surface quality of workpiece with respect to surface profile and roughness during the precision end-milling process. Singular spectrum analysis (SSA) is a new non-parametric technique of time series analysis and forecasting. The significant features of the cutting tool vibration signals from the sensors are extracted and transformed from the SSA-processed vibration signals. In the present study, SSA is applied to extract and transform the raw signals of the vibrations on the cutting tool for investigating the relationship between tool vibration and surface roughness in the precision end-milling process of hardened steel SCM440. In this experimental investigation, the spindle speed, feed rate, and cutting depth were chosen as the numerical factor; the cutting feed direction and holder type were regarded as the categorical factor. An experimental plan consisting of five-factor (three numerical plus two categorical) D-optimal design based on the response surface methodology was employed to carry out the experimental study. A micro-cutting test was conducted to visualize the effect of vibration of tooltip on the performance of surface roughness. With the experimental values up to 95% confidence interval, it is fairly well for the experimental results to present the mathematical models of the tool vibration and surface roughness. Results show that the effects of feed rate and cutting depth provide the reinforcement on the overall vibration to cause the unstable cutting process and exhibit the result of the worst machined surface. The amplitude of vibration signals along the cutting feed direction is generally larger than that along other direction. The spindle speed and tool holder type affect the stability of cutting tooltip during the cutting process.

Keywords Vibration · Surface roughness · Precision end milling · Singular spectrum analysis

C.-C. Chen
Department of Mechanical and Automatic Engineering,
Chungchou University of Science and Technology,
No.6, Lane 2, Sec. 3, Shanjiao Rd., Yuanlin Town,
Changhua, Taiwan 51001, Republic of China
e-mail: jcchen@dragon.ccut.edu.tw

N.-M. Liu · K.-T. Chiang (✉) · H.-L. Chen
Department of Mechanical Engineering,
Hsiuping University of Science and Technology,
No. 11, Gungye Rd., Dali District,
Taichung, Taiwan 41280, Republic of China
e-mail: kota@hit.edu.tw

K.-T. Chiang
e-mail: vgear2001@yahoo.com.tw

N.-M. Liu
e-mail: nunming58@yahoo.com.tw

N.-M. Liu
e-mail: nunming58@gmail.com

H.-L. Chen
e-mail: chl9265@yahoo.com.tw

1 Introduction

In precision machining operation, the surface finish of high quality is an important requirement for many manufactured products. The exact degree of surface finish is a considerable important factor affecting the function and the cost of products in the field of manufacturing industry, especially for the highly durable molds of complex and precise components. The mechanism of surface roughness formation depends on various uncontrollable factors. The cutting conditions of machining operation, including the cutting speed, feed rate, depth of cut, tool geometry, and the material properties of both the tool and workpiece, have been reported

to be fairly strongly correlated with the surface finish quality of machined parts [1]. During the machining process, the relative vibration condition, occurring among the instrument, cutting tool, chuck, and workpiece, is an inextricable part and it has detrimental effects on the quality of machined surface [2]. Especially, the relative vibrations of cutting tool and workpiece cause the poor-machined surface roughness, poor dimensional accuracy of the workpiece and abnormal tool wear or tool breakage, which lowers down the productivity and increases the cost of production. The appearance of vibrations on the cutting tools is mainly subjected to the cutting dynamics process under various cutting conditions. The dynamic phenomena of cutting tool induced by the interaction of elastic system in the cutting process causes the relative displacement between tool and workpiece, which generates the vibration of the cutting tool [3, 4]. Moreover, the major detrimental effect of vibration for the workpiece further worsens the quality of the machined surface. Surface roughness has been widely used in the index of the machined surface quality since a reasonably good surface finish was good for improving the tribological properties, fatigue strength, corrosion resistance, and esthetic appeal of the machined product [5, 6]. Excessive vibration can also cause the damage on the cutting tool and interfere with the feed rate, cutting speed, and cutting depth.

The amplitude and natural frequency of cutting tool vibrations under the resonance during cutting process are related to the dynamic cutting force and the chip-thickness variation acting on the cutting tool. The variation of cutting tool vibrations in the finish cutting process is observed through the monitor of surface roughness growth on the machined surface. In the past efforts, most researches was reported in the literature focusing on using the virtual vibration signals to analyze the effects of cutting tool vibrations on the machined surface, and proposed the predicted vibrations model which are determined by the cutting process dynamics. Mer and Diniz [7] carried out the experiments for correlating the variation of the tool vibration, tool wear, tool life, and surface roughness in the finish turning with the coated carbide tools. Thomas et al. [6] investigated the effect of cutting tool vibrations on surface roughness during the lathe dry turning of mild carbon steel under different cutting parameters including the cutting speed, feed rate, cutting depth, tool nose radius, tool overhang, and workpiece length. Jang et al. [8] proposed a measuring technique of online real-time roughness, which is a monitoring algorithm dealing with the relative cutting vibrations between tool and workpiece, so as to study the correlation between surface roughness and cutting vibration in hard turning process. Abouelatta and Madl [9] proposed the mathematical prediction model of surface roughness based on cutting parameters and tool vibrations in turning operations. Dimla [10] described a tool-wear monitoring procedure in a metal-turning operation using vibration features. The monitoring procedure revealed that the vibration signals' features are related to the wear qualification of cutting tool wear. Risbood et al. [11] utilized the fitted network for predicting the surface finish and dimensional deviation by measuring cutting forces and vibrations in the turning process. Li et al. [12] made an experimental study of tool wear and cutting force variation in the end milling of Inconel 718 with coated carbide inserts. Consequently, the various features of cutting tool vibration signals have been chosen to estimate surface quality.

The measuring technology of cutting tool vibrations relies on three steps: (1) selection of sensors, (2) extraction and transformation of significant features of the raw vibration signals from the sensors, and (3) classification of the collected raw vibration signals so as to identify the quantitative estimation of vibration signals and development of a decision strategy in controlling the machining process. The significant features of the cutting tool vibration signals from the sensors are extracted and transformed from the singular spectrum analysis (SSA)-processed vibration signals [13]. SSA is a new non-parametric technique of time series analysis and forecast. Alonsoa and Salgadob [14] developed a reliable tool condition monitoring system which based on the analysis of the structure of the tool vibration signals using SSA and cluster analysis. Kilundu et al. [15] utilized SSA as signal processing tool for dealing with non-stationary vibrations recorded in metal cutting process.

In this present work, an attempt had been made to investigate the relationship between the tool vibration and surface roughness in the precision end-milling process. A micro-cutting test is conducted to visualize the effect of cutting tool vibrations on the performance of surface roughness. The raw signals of cutting tool vibrations are extracted and transformed using the technology of SSA. The evaluation of machinability performances adopts the surface roughness to identify the quantitative estimation of cutting tool vibrations under various cutting conditions. This experiment adopted the harden chromium–molybdenum steel (SCM440) as experimental specimen. In this experimental investigation, the spindle speed, feed rate, cutting depth were chosen as the numerical factor; the cutting feed direction and holder type were regarded as the categorical factor. A five-factor (three numerical plus two categorical) D-optimal design based on the response surface methodology (RSM) is employed to determine the experimental runs for the operating conditions of cutting process. Myers and Montgomery [16] and Khuri and Cornell [17] offered the practical applications of RSM which is a statistical modeling approach to determine the relationship between various process parameters and responses with the various desired criteria, and further to search the significance of these process parameters on the

coupled responses. Consequently, the RSM is utilized to describe and identify, with a great accuracy, the influence of the interactions between different variables on the response when they are varied simultaneously [18–23]. The D-optimal design concept for non-linear models was first introduced by Box and Lucas [24], which represents a specific illustration of two sequential chemical reactions. The D-optimal design is verified to provide the best possible design for the smallest possible confidence intervals on the estimated model parameters. In this paper, a mathematical model based on the response surface-based D-optimal design is proposed for modeling and analyzing the tool vibration and surface roughness in the precision end-milling process.

2 Singular spectrum analysis

SSA is an on-parametric technique of time series analysis and forecast based on principles of multivariate statistics. Its technique combines the elements of classical time series analysis, multivariate statistics, multivariate geometry, dynamical systems, and signal processing. It decomposes the original series into the sum of a small number of independent and interpretable components such as a slowly varying trend, oscillatory components, and a structural noise. The basic SSA algorithm comprises two stages: the decomposition of a time series and the reconstruction of a desired additive component.

The decomposition stage requires a embedding and singular value decomposition (SVD). The process that a matrix is called the trajectory matrix built from the original time series is called the embedding. The trajectory matrix consists of vectors obtained by means of a sliding window that traverses the series. In the embedding step, let $X=(x_1, x_2,\ldots, x_N)$ be the time series of length N to be analyzed, and a given integer denominated to be window length L with $1<L<N$. The time series X are mapped into the L and lagged vectors $X_i = (x_i, x_{i+1}, ..., x_{i+L-1})^T$ for $i=1, 2,\ldots, K$, where $K=N-L+1$, with which one constructs the trajectory matrix $X=(X_1, X_2,\ldots, X_K)$ of size $L\times K$. The trajectory matrix X is a Hankel matrix in which cross-diagonals elements x_{i+j-1}=constant and are equal.

$$X = \begin{bmatrix} X_1 \\ X_2 \\ \vdots \\ X_K \end{bmatrix} = \begin{bmatrix} x_1 & x_2 & \cdots & x_L \\ x_2 & x_3 & \cdots & x_{L+1} \\ \vdots & \vdots & \ddots & \vdots \\ x_K & x_{K+1} & \cdots & x_N \end{bmatrix} \tag{1}$$

Afterwards, the SVD step makes the singular value decomposition of the trajectory matrix X and provides the collection of eignevalues and eigenvalues of the matrix $S=X\times X^T$ of size $L\times L$. Let $\lambda_1, \lambda_2\ldots, \lambda_d$ be the non-zero eignevalues of S, and $U_1, U_2,\ldots, U_d$ be the corresponding eigenvectors, in which $d=\max(i : \sqrt{\lambda_i} > 0)$. A decomposition of the trajectory matrix X is obtained into a sum of matrices

$$\begin{aligned} X &= T_1 + T_2 + \cdots + T_d \\ &= U_1\sqrt{\lambda_1}V_1^T + U_2\sqrt{\lambda_2}V_2^T + \cdots + U_d\sqrt{\lambda_d}V_d^T \\ &= \sum_{i=1}^{d} U_i\sqrt{\lambda_i}V_i^T \end{aligned} \tag{2}$$

where the vector $V_i = X^T \times U_i/\sqrt{\lambda_i}$. The plot of the eigenvalues in decreasing order is call the *singular spectrum* which presents the weight of the norm of each elementary matrix in the norm of the trajectory matrix.

The reconstruction stage transforms from a $L\times K$ matrix into a time series of length N using the grouping and the diagonal averaging. The grouping step corresponds to splitting the elementary matrices T_I into several groups and summing the matrices within each group. The grouping step is a partition of the set of indices 1, 2,…, d into the collection of m disjoined subsets of $I=(I_1, I_2,\ldots, I_m)$. The matrix T_I corresponds to the group $I=(I_1, I_2,\ldots, I_m)$. So the trajectory matrix X can be expanded as

$$X = T_{I_1} + T_{I_2} + ... + T_{I_d} \tag{3}$$

The diagonal averaging algorithm obtains the reconstructed time series $\widetilde{T}$ from the averaging of the corresponding diagonals of the matrix T_{I_i}.

$$\widetilde{T} = \begin{cases} \frac{1}{s-1}\sum_{j=1}^{s-1} x_{j,s-j} & \text{for } 2 \le s \le L \\ \frac{1}{L}\sum_{j=1}^{L} x_{j,s-j} & \text{for } L+1 \le s \le K+1 \\ \frac{1}{N-s+2}\sum_{j=s-K}^{N-s+2} x_{j,s-j} & \text{for } K+2 \le s \le N+1 \end{cases} \tag{4}$$

3 Experimental design and procedure

3.1 Experimental setup

In this study, the experimental setup for the precision end-milling experiments is shown in Fig. 1. All the micro-cutting experiments were conducted without any coolant in an EMV-600 vertical machining center, which has a maximum spindle speed of 8000 rpm, machining table size 700×450 mm and 16 tools armless type automatic tool change, a simplified magazine construction. The workpiece material used in this study is the hardened SCM440 and heat treated to R_c 60 with the following chemical compositions in mass percent: 0.38~0.43 C, 0.15~0.35 Si, 0.60~0.85 Mn, 0.03 P

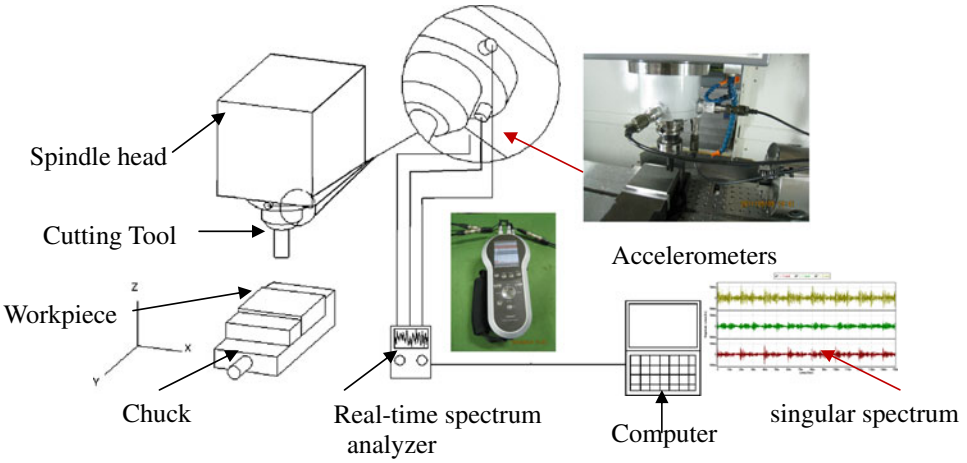

Fig. 1 Schematic diagram of the experimental setup

max, 0.03 S max, 0.03 Cu max, 0.25 Ni max, 0.90~1.20 Cr, 0.15~0.30 month and bal. Fe. This material has an ultimate tensile strength of at least 95 MPa and yield strength of at least 75 MPa, commonly used for the high toughness machinery components such as the rotating shafts, gear, crankshaft, etc. Before micro-cutting, each experimental specimen was cut as a rectangular block. The metal cutting process was designed and machined by using Solidworks CAD/CAM software. The completion and positioning of cutting process were machined and controlled by using CNC software.

Type ACP200 AXMT123508 PEER-G tool inserts made by Sumitomo Electric Inc. were employed in the experiments. The surface of cutting tool inserts was deposited with physical vapor of TiAlN and AlCrN. Two types of tool holder are FMDX-1734-S (A type) and FMDX-2142-S (B type), as shown in Fig. 2. The former holder has two tool inserts, and the latter has three.

The monitoring system of cutting condition is composed of data acquisition system. The data acquisition system consists of three signal measurement sensors (accelerometer) and a singular spectrum analysis (SSA) device. In order to detect the vibration condition in the turning process, the vibration signals were measured using three 353B16 ICP accelerometers that was placed next to the cutting tool and sensed the vibration in the *X*-axial, *Y*-axial, and *Z*-axial direction, respectively. The vibration signals along the cutting path direction was found to be highly sensitive to the performance of roughness on the machined surface. The sensitivity of the accelerometer was 10 mV/g (±15%), and its measurement range was 0.7~20 kHz. These sensed vibration signals collected in the time domain were then sent to the SSA device for the calculation of root mean square (RMS) value of vibration signal for each experiment. The RMS value of vibration signal represents the square root of the average of the squared value of the vibration amplitude. Therefore, the vibration signals acquired through the accelerometer were extracted and transformed by the SSA device for the analysis of frequency domain. The procedure of SSA decomposes a given time series into a set of independent additive time series according to the content in the Section 2. The main function of singular spectrum analyzer is to represent the spectrum characteristics of a given time series signal in the frequency domain. When the cutting operation is in process, the sensors dynamically collect the raw vibration signals. These vibration signals obtained in time domain are transformed to frequency domain by the fast Fourier transform (FFT). The power spectrum density analysis is performed according to the output of FFT. The vibration signals called

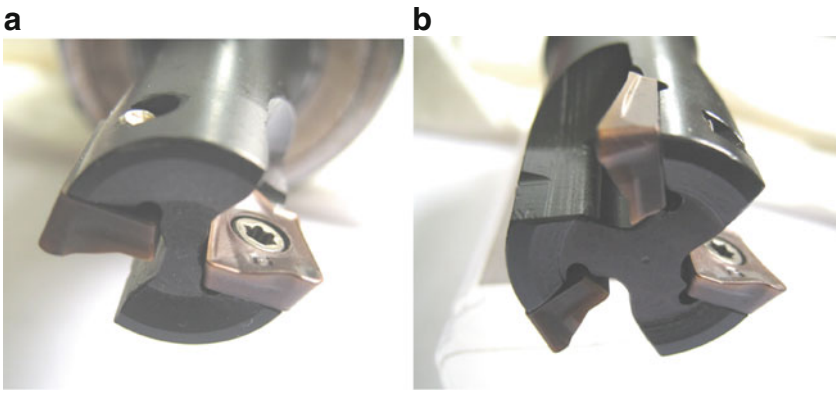

Fig. 2 Two types of tool holders: **a** FMDX-1734-S (A type) and **b** FMDX-2142-S (B type)

spectrum in the frequency domain were analyzed for different cutting processes. In the experimental setup, the singular spectrum analyzer is a real-time spectrum analyzer (four channel real time analyzer, G-Tech Instrument Inc.) which displays the singular amplitude of frequency domain immediately. The measured signal bandwidth was set as 1 kHz.

3.2 Experimental design

In the real end-milling process, the cutting length, and size of experimental specimen were kept the same so that no further vibrations are induced by the deflection of workpiece. The cutting length and size of experimental specimen were fixed at 80 mm (millimeter) and $100\times100\times32$ mm^3 in the experimental design, respectively. In order to visualize the effect of cutting tool vibrations on the surface roughness, a micro-cutting test is conducted as follows. The spindle speed (N) was varied from 3,000 to 5,000 rpm; the feed rate (f) were changed between 100 and 300 mm/rev, and the cutting depth (α_P) were set from 0.1 to 0.3 mm. The cutting feed path adopted X-axial and Y-axial direction to compare and identify the vibration effect induced by spindle header. Table 1 shows the setting of experimental parameters and instrument under cutting the hardened SCM440 steel in the precision end-milling process.

In the present study, the frequency and amplitude of vibration signals were considered as the criterion and would affect the machinability evaluation in the precision end-milling process. The value of surface roughness here was adopted as the machinability evaluation of hardened SCM440 steel machined in the precision turning process. The measurements of the surface roughness for the machined surface were performed by using a Mitutoyo SurfTest-402 with a cut-off length of 80 mm (millimeter) and sampling length of 60 mm (millimeter). The maximum surface roughness (R_{max}) was used to evaluate the surface roughness of the machined surface. The frequency and amplitude in the power spectrum density plots of the vibration signals were recorded to identify the quantitative estimation of cutting tool vibrations under various cutting conditions. In the precision turning process, the lower both amplitude of vibration signals and surface roughness (R_{max}) are, the better the indication of the response characteristics. Those desired responses are regarded as the smaller-the-better characteristics and influence each other relatively.

Table 1 Experimental parameters and instrument

Working conditions		Unit	Description
Miller			EMV-600 CNC
Workpiece			SCM-440 S6
Holder type	A type		F MDX-1734-S
	B type		FMDX-2142-S
Insert type			ACP 200 AXMT 123508 PEER-G
Cutting length		mm	100
Spindle speed (N)		rpm	3,000–5,000
Feed rate (f)		mm/rev	100–300
Cutting depth (α_P)		mm	0.1–0.3
Cutting feed direction			X-axial and Y-axial direction
Cooling Liquid			Dry
Accelerometers			353B16 ICP
Data acquisition			Real-time spectrum analyzer

A-type holder has two inserts, and B type has three inserts

According to the previous analysis in the real cutting process, the spindle speed (N), the feed rate (f), and the axial depth of cut (α_P), were actually chosen as the three numerical factors for investigation. The cutting feed direction was adopted along the X-axial and Y-axial directions. The status of tool holder type sets up two categories including the A type and B type during the cutting process. It displays that the number of tool inserts would affect the continuity of cutting force. The status of cutting feed direction and tool holder type were regard as the categorical factor. Table 2 shows the controllable parameters and their levels in the coded and actual values.

The experimental matrix adopted in this study in the coded form is shown in Table 3. The coded values $X_{i,i=1,2,3}$ of the numerical factors used in Tables 2 and 3 were obtained from the following transformable equations:

$$X_1 = \frac{N - N_0}{\Delta N} \tag{5}$$

$$X_2 = \frac{f - f_0}{\Delta f} \tag{6}$$

$$X_3 = \frac{\alpha_P - \alpha_{P0}}{\Delta \alpha_P} \tag{7}$$

where X_1, X_2, and X_3 are the coded values of parameters N, f, and α_P, respectively. N_0, f_0, and α_{P0} are the values of N, f, and α_P at zero level. ΔN, Δf, and $\Delta\alpha_P$ are the intervals of variation in N, f, and α_P, respectively. The coded value X_4 represents the status of cutting feed direction including the X-axial direction (X_4=1) and Y-axial direction (X_4=2), respectively. The coded value X_5 represents the status of tool holder type including the A type (X_5=1) and B type (X_5=2), respectively.

Table 2 Design schema of machining parameters and their levels

Machining parameters	Unit	Code		Levels				
				1	2	3	4	5
			Numerical	−2	−1	0	+1	+2
			Categorical	1	2			
Spindle speed (N)	rpm	X_1		3,000	3,500	4,000	4,500	5,000
Feed rate (f)	mm/rev	X_2		100	150	200	250	300
Cutting depth (α_P)	mm	X_3		0.10	0.15	0.20	0.25	0.30
Cutting feed direction		X_4		X-axial	Y-axial			
Holder type		X_5		A	B			

Table 3 Design layout and experimental results

Run	Coded factors					Actual factors					Responses			
	Spindle speed	Feed rate	Cutting depth	cutting feed direction	Tool holder type	Spindle speed	Feed rate	Cutting depth	Cutting feed direction	Tool holder type	Roughness	Vibration amplitude		
	X_1	X_2	X_3	X_4	X_5	N	f	α_P			R_{max} (Y_1 μm,)	X-axial (Y_2, mGs)	Y-axial (Y_3, mGs)	Z-axial (Y_4, mGs)
1	0	−2	−2	2	1	4000	100	0.1	Y	A	0.28	92.2	109.1	176.4
2	+2	−2	−2	1	1	5000	100	0.1	X	A	0.14	45.6	58.5	84.2
3	+2	−2	+2	2	1	5000	100	0.3	Y	A	0.45	148.6	172.7	268.5
4	−2	−2	0	2	1	3000	100	0.2	Y	A	0.22	71.6	87.9	139.7
5	0	−2	−2	2	1	4000	100	0.1	Y	A	0.35	116.2	137.1	212.2
6	−2	+2	+2	2	1	3000	300	0.3	Y	A	0.49	159.6	189.2	291.2
7	+1	+1	+1	1	2	4500	250	0.25	X	B	0.34	110.7	143.8	208.1
8	+2	+2	−2	2	1	5000	300	0.1	Y	A	0.3	97.7	125.8	178.3
9	+2	+2	+2	1	1	5000	300	0.3	X	A	0.26	86.7	107.9	156.5
10	+2	−2	−2	2	2	5000	100	0.1	Y	B	0.26	84.2	101.4	148.5
11	−2	0	−2	2	1	3000	200	0.1	Y	A	0.44	144.3	171.9	264.5
12	−2	0	−2	2	1	3000	200	0.1	Y	A	0.44	143.9	169.9	261.5
13	+2	−2	−2	2	2	5000	100	0.1	Y	B	0.26	84.7	102.6	156.5
14	−2	−2	+2	2	2	3000	100	0.3	Y	B	0.38	123.8	146.7	227.9
15	+1	−1	−1	1	2	4500	150	0.15	X	B	0.28	91.2	112.6	168.4
16	−2	+2	−2	2	2	3000	300	0.1	Y	B	0.4	130.3	157.4	238.7
17	+2	−2	+2	1	2	5000	100	0.3	X	B	0.31	101	121.2	186.2
18	−2	−2	0	2	1	3000	100	0.2	Y	A	0.22	72.6	86.9	132.7
19	−2	−2	−2	1	2	3000	100	0.1	X	B	0.27	87.9	116.7	161.5
20	0	0	0	1	1	4000	200	0.2	X	A	0.21	68.4	85.6	125.8
21	−2	+2	+2	1	2	3000	300	0.3	X	B	0.54	176.9	213.6	321.5
22	+2	+2	+2	1	2	5000	300	0.3	Y	B	0.35	115.7	137.1	209.7
23	−1	+1	−1	1	2	3500	250	0.15	X	B	0.31	102.3	121.2	185.2
24	−2	−2	+2	1	1	3000	100	0.3	X	A	0.29	112.7	97.5	173.4
25	+2	+2	+2	2	2	5000	300	0.3	Y	B	0.35	116.3	137.2	208.2
26	−2	+2	−2	1	1	3000	300	0.1	X	A	0.26	84.7	103.9	152.5
27	+2	+2	−2	1	2	5000	300	0.1	X	B	0.17	65.3	67.1	101.5
28	+1	+1	+1	2	1	4500	250	0.25	Y	A	0.35	115.3	136.1	208.7
29	−1	0	0	2	2	3500	200	0.2	Y	B	0.29	94.5	112.4	172.4

3.3 D-optimal design of the response surface methodology

A response surface-based D-optimal design was used to determine the experimental runs for the operating conditions of cutting process. The procedures of D-optimal design consist of the defining level, selection of the fitting model and the chosen design points. The design points chosen from the set of candidate points depend on the selected model. As presented in Table 2, three numerical factors are varied over five levels, while two categorical factors are at two categories. In this study, the quantitative form of relationship between the desired response and independent input variables can be represented in the following:

$$Y = f(X_1, X_2, X_3, X_4, X_5) \tag{8}$$

where Y is the desired response and f is the response function (or response surface). In this particular case, the approximation of Y was proposed by using the fitted second order polynomial regression model which is called the quadratic model. The quadratic model was exactly suitable for studying carefully the interactive effects of combinative factors on the performance evaluations. The quadratic model of Y can be written as follows:

$$Y = a_0 + \sum_{i=1}^{5} a_i X_i + \sum_{i=1}^{5} a_{ii} X_i^2 + \sum_{i<j}^{5} a_{ij} X_i X_j \tag{9}$$

where a_0 is constant, a_i, a_{ii}, and a_{ij} represent the coefficients of linear, quadratic, and cross-product terms, respectively. This model using the quadratic model of f in this study not only aims to investigate the response over the entire factor space, but also to locate the region of desired target where the response approaches to its optimum or near optimal value. In general, the quadratic model of desired response (Y) can be expressed in the matrix form as follows:

$$Y = X\alpha + \varepsilon \tag{10}$$

where $\mathbf{X}$ is a matrix of model terms evaluated at the data points, ε is an error vector. The unbiased estimator ε of the regression coefficient vector α is estimated by using the least-squares error method as follows.

$$\alpha = \left(X^T X\right)^{-1} X^T Y \tag{11}$$

where $\mathbf{X^T}$ is the transpose of the matrix $\mathbf{X}$.

The algorithm of D-optimal design for choosing design points is to select the set of design points by the selected quadratic model, which results in 19 minimum model points, and 5 points of them are used to estimate the lack-of-fit and replicates as well. The 29 experimental runs based on D-optimal design were performed to provide the suitable framework for this cutting experimentation, as shown in Table 3. It also displays the run numbers and the observed responses. Each cutting experiment was carried out two times at different time under the same conditions to ensure that the experimental data were repeatable.

4 Results and discussion

4.1 Identification of cutting tool vibration

For identifying the elastic deformations of the MFTW (machine-fixture-tool-work) system and their influence under the no cutting condition, the power spectrum density plots and the vibration amplitudes in the X-axial, Y-axial, and Z-axial direction of the cutting tool were collected. These sensed vibration signals collected in the time and frequency domain were regarded as the basic reference to compare the quantitative estimation of cutting tool vibrations under various cutting conditions. This process is to identify the dynamic parameters of the MFTW system such as system damping and stiffness in standstill under various cutting conditions. It is essential for time domain signal analysis to understand the overall vibration level generated in cutting process. The vibration raw signals of the X-axial, Y-axial, and Z-axial direction on the cutting tool were recorded within 150 ms. Figure 3 reveals the vibration amplitudes in the X-axial, Y-axial, and Z-axial direction of the cutting tool under the standstill and idle running conditions. The idle running condition sets up the status of spindle speed to be 5,000 rpm. It shows that the trend of vibration signals amplitude under the standstill condition is similar to under the idle running condition. From the visualized time domain vibration data, the average values of vibration signals amplitude are 2.917, 4.006, and 4.117 mGs in the X-axial, Y-axial, and Z-axial direction, respectively. The power spectrum density plots of other vibration signals in the frequency domain under the standstill and idle running conditions are shown in Fig. 4. It is observed that the characteristics of the peaks appear at the frequency within 0~4 kHz and these peaks are regarded as the excited natural frequency induced by the structure of machine. It also shows that the trend of these peaks under the standstill condition is similar to under idle running condition. Consequently, these results were to identify the dynamic parameters of MFTW system such as system damping and stiffness under the standstill and idle running conditions.

When the material of workpiece was cut, large amplitude vibrations induced by cutting force were generated on the cutting tool, especially in the cutting feed direction. Figure 5 reveals the vibration amplitudes in the X-axial, Y-axial, and Z-axial direction of the cutting tool under the dry cutting conditions. The dry cutting condition employs the cutting parameter setup of spindle speed of 3,000 rpm, feed rate of 100 mm/rev, cutting depth of 0.10 mm, and X-axial cutting feed direction. In real end-milling process, the material of

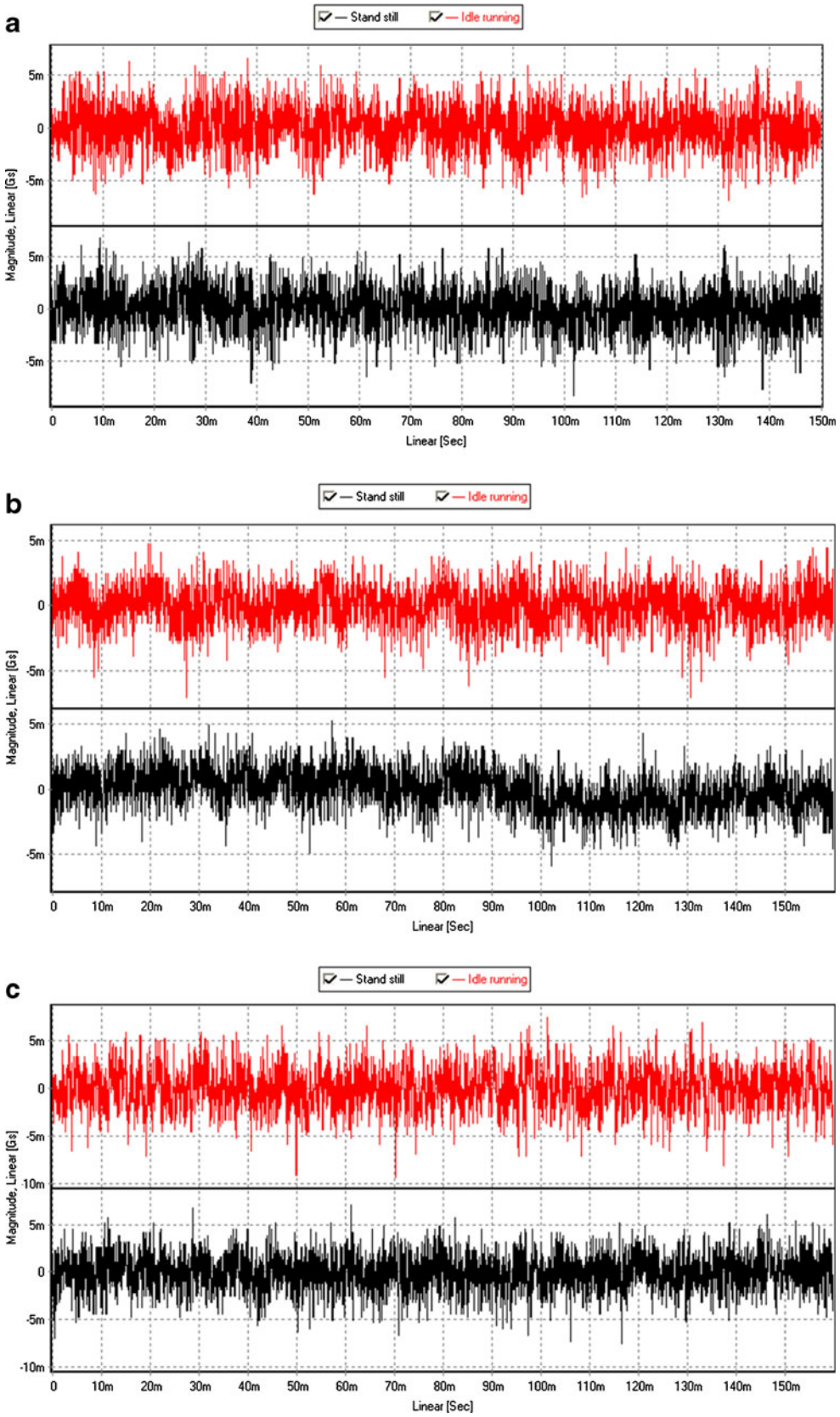

Fig. 3 The vibration amplitude of **a** *X*-axial, **b** *Y*-axial, and **c** *Z*-axial direction on the cutting tool under the standstill and idle running conditions

workpiece is fed into a rotating multi-point cutting tool. Under non-steady-state and cyclic conditions, the varying cutting forces during the contact of the cutting edge will result in the variation of chip thickness. Under these

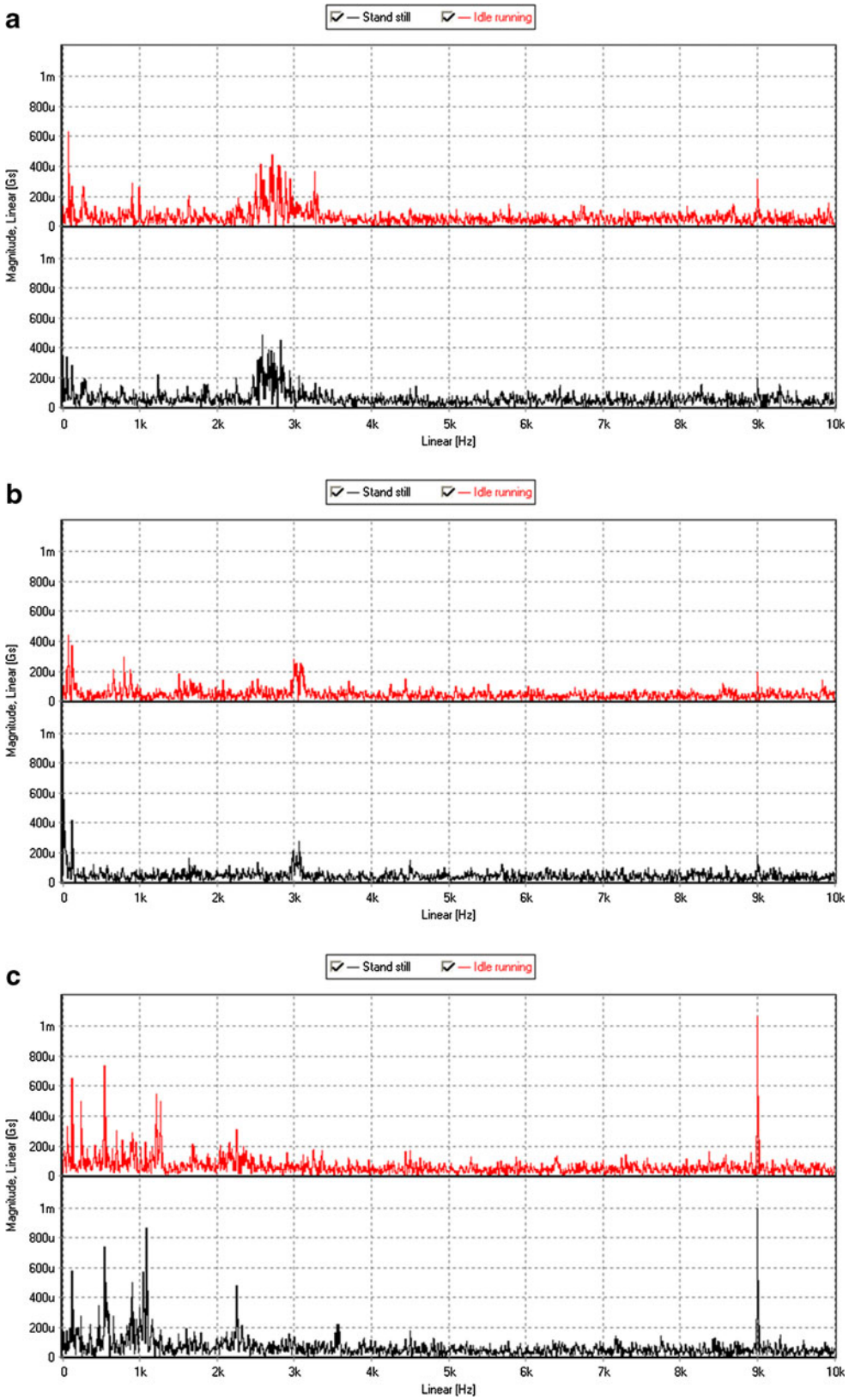

Fig. 4 The power spectrum of the cutting tool under the standstill and idle running conditions in **a** *X*-axial, **b** *Y*-axial, and **c** *Z*-axial direction, respectively

conditions, the varying cutting forces can easily excite the natural frequency of the MFTW system and is harmful to the tool life and surface finish generated. From Fig. 5, it reveals that the change of the vibration amplitudes is obviously performed in the cutting process. However, comparing the amplitudes shown in Fig. 5, it can be found that the

dominant spectrum peaks of vibration signals amplitude in the *Z*-axial direction of the cutting tool are larger than those in the *X*-axial and *Y*-axial directions. The vibration induced by the non-steady-state cyclic conditions of the varying cutting forces can be significant validation in the *Z*-axial direction of the cutting tool. It can be observed that the average values of vibration signals amplitude are about 110.0, 93.9, and 171.9 mGs in the *X*-axial, *Y*-axial, and *Z*-axial direction, respectively. In the precision end-milling process, the vibration stability of cutting tool affects the quality of the machined surface. The status of vibration signals amplitude corresponds to the amount of unstable conditions acting on the tip of cutting tool. These amplitudes present the status of the relative movement between the cutting tool and workpiece, and are regarded as dominant factors affecting the surface roughness.

The power spectrum density plots of these vibration signals along the *X*-axial, *Y*-axial, and *Z*-axial direction in the frequency domain are shown in Fig. 6. It is observed that the dominant spectrum peaks appear at the frequency within 2~4 kHz in the *X*-axial and *Y*-axial direction of the cutting tool during the real end-milling process. The frequencies of the characteristic peaks at the high-frequency band (above 5 kHz) are found to be not very sensitive to the cutting conditions. But, the dominant spectrum peaks along the *Z*-axial direction of the cutting tool appeared at the low frequency band of 0.5~1.5 kHz. It was caused by the interaction between the tooltip and the elastic recovery induced by the feed force of cutting tool.

4.2 The analysis of the proposed quadratic mathematical model

The 29 experimental runs were conducted in duplicate, and the average values of surface roughness (Y_1, micrometers), *X*-axial vibration amplitude (Y_2, milligauss), *Y*-axial vibration amplitude (Y_3, milligauss), and *Z*-axial vibration amplitude (Y_4, milligauss) along with the design matrix are listed in Table 3.

In order to ensure the goodness of fit of the mathematical quadratic model obtained in this study, the test for significance of the regression model, the test for significance on individual model coefficients and the test for lack-of-fit need to be performed [16, 17] as shown in Table 4. These tests are performed as analysis of variance (ANOVA) procedure by calculating the "*F* value", the "Prob.>*F*", the determination coefficients (R^2), adjusted *R*-squared (R^2-adjusted), and the adequate precision (AP). The values of "*F* value" and the "Prob.>*F*" imply a statistical significance on the regression model and the particular linear, quadratic, or interaction terms. Usually as the desired confidence level is set to 95%, the value of "Prob.>*F*" smaller than 0.05 signifies that the regression model is considered to be statistically significant, which is desirable as it demonstrates that the terms in the model have a significant effect on the responses. The determination coefficient R^2 is defined as the ratio of the explained variation to the total variation and is a measure of the degree of fit. When the value R^2 approaches to unity, the better the response model fits the actual data, the less the difference between the predicted and actual values exists. The adjusted *R*-squared (R^2-adjusted) presents a measure of the amount of variation around the mean explained by the model, adjusted for the number of terms in the model. The adjusted *R*-squared (R^2-adjusted) decreases as the number of terms in the model increases if those additional terms do not add value to the model. Furthermore, the value of AP in this model, which compares the range of the predicted value at the design point to the average prediction error, is well above 4. The value of the ratio is greater than 4, which presents the adequate model discrimination. These models obtain higher values of the R^2, R^2-adjusted, and AP at the same time.

From the results of Table 4, the obtained quadratic mathematical models for the responses Y_1 (surface roughness,

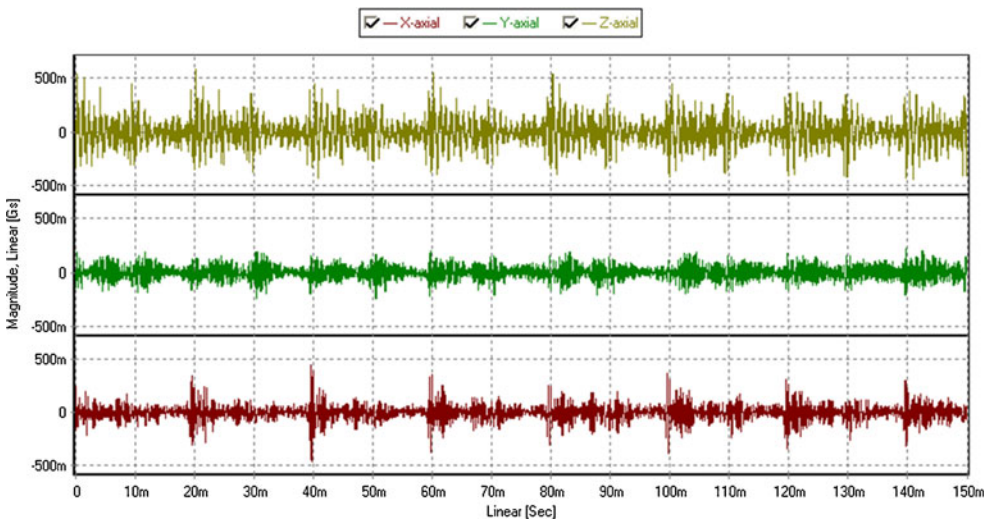

Fig. 5 The vibration amplitude of *X*-axial, *Y*-axial, and *Z*-axial direction on the cutting tool under the dry cutting conditions

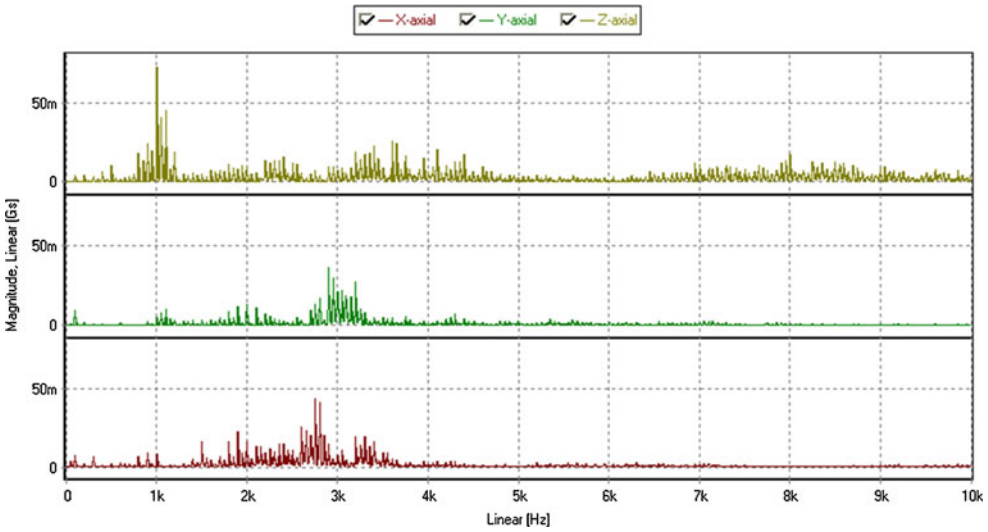

Fig. 6 The power spectrum of *X*-axial, *Y*-axial, and *Z*-axial direction on the cutting tool under the dry cutting conditions

micrometers), Y_2(*X*-axial vibration amplitude, milligauss), Y_3 (*Y*-axial vibration amplitude, milligauss), and Y_4 (*Z*-axial vibration amplitude, milligauss) can be regarded as significant effect for fitting and predicting the experimental results and meantime the test of lack-of-fit also displays to be insignificant.

Table 5 shows that the values of "*F* value"' and "Prob.>F" for each term on the performances of the obtained quadratic mathematical models. The terms can be regarded as significant terms due to their "Prob.>*F*" values are less than 0.05. The backward elimination process eliminates the insignificant terms to adjust the fitted quadratic models. These insignificant model terms can be removed and the test of lack-of-fit also displays to be insignificant. Through the backward elimination process, the final quadratic models of response equation in terms of coded factors are presented as follows:

$$Y_1 = 0.2801 - 0.0385X_1 + 0.0215X_2 + 0.0591X_3 - 0.0365X_4 + 0.0138X_5 - 0.0892{X_2}^2 + 0.1339{X_3}^2 - 0.0344X_1X_2 - 0.0335X_4X_5 \quad (12)$$

$$Y_2 = 103.6052 - 13.0439X_1 + 8.2089X_2 + 3.1444X_3 + 6.7644X_4 + 0.0138X_5 - 29.2985{X_2}^2 + 42.5610{X_3}^2 - 12.2615X_1X_2 - 6.4822X_1X_5 - 13.6264X_4X_5 \quad (13)$$

$$Y_3 = 112.9526 - 112.9526X_1 + 13.6081X_2 + 20.8377X_3 + 14.1051X_4 + 6.2551X_5 - 33.2635{X_2}^2 + 48.7115{X_3}^2 - 12.6395X_1X_2 - 7.18057X_1X_5 - 14.2708X_4X_5 \quad (14)$$

$$Y_4 = 180.8447 - 25.6075X_1 + 10.7889X_2 + 33.3734X_3 + 21.2924X_4 + 4.5278X_5 - 58.2459{X_2}^2 + 72.3312{X_3}^2 - 18.8073X_1X_2 + 5.4720X_1X_4 \quad (15)$$

Table 4 Results of the ANOVA for the fitted models

Final quadratic models	Surface roughness, R_{max} (Y_1)	*X*-axial vibration amplitude (Y_2)	*Y*-axial vibration amplitude (Y_3)	*Z*-axial vibration amplitude (Y_4)
F value	14.37	10.64	10.18	14.09
Prob.>*F*	<0.0001	0.0003	0.003	<0.0001
R^2	0.928	0.950	0.948	0.962
R^2-adjusted	0.895	0.861	0.855	0.893
Adequate precision (AP)	16.048	15.640	13.767	15.956
Lack-of-fit	Not significant	Not significant	Not significant	Not significant

Table 5 Results of the ANOVA

Symbol	Surface roughness, $R_{max}(Y_1)$		*X*-axial vibration amplitude (Y_2)		*Y*-axial vibration amplitude (Y_3)		*Z*-axial vibration amplitude (Y_4)	
	F value	Prob.>*F*	*F* value	Prob.>*F*	*F* value	Prob.>*F*	*F* value	Prob.>*F*
$X_1(N)$	32.974	0.0002[a]	25.043	0.0005[a]	20.447	0.0011[a]	33.040	0.0002[a]
$X_2(f)$	9.147	0.0128[a]	8.976	0.0134[a]	9.422	0.0118[a]	8.219	0.0168[a]
$X_3(\alpha_P)$	72.283	<0.0001[a]	54.190	<0.0001[a]	43.239	<0.0001[a]	72.373	<0.0001[a]
X_4	36.582	0.0001[a]	0.683	0.4278	23.447	0.0007[a]	36.042	0.0001[a]
X_5	5.379	0.0428[a]	8.128	0.0172[a]	5.283	0.0444[a]	5.214	0.0455[a]
X_1^2	0.037	0.8495	0.265	0.6177	0.221	0.6478	0.002	0.9645
X_2^2	18.985	0.0014[a]	11.801	0.0064[a]	11.438	0.0070[a]	17.018	0.0021[a]
X_3^2	34.1	0.0002[a]	18.435	0.0016[a]	18.996	0.0014[a]	33.295	0.0002[a]
X_1X_2	19.855	0.0012[a]	16.259	0.0024[a]	13.615	0.0042[a]	17.995	0.0017[a]
X_1X_3	0.0350	0.8552	0.710	0.4189	0.365	0.5587	0.102	0.7556
X_1X_4	4.071	0.0713	3.974	0.0742	2.485	0.1460	3.138	0.1069
X_1X_5	4.27	0.0657	6.582	0.0281[a]	6.089	0.0332[a]	4.182	0.0681
X_2X_3	0.316	0.5861	2.5324	0.1426	1.236	0.2922	0.394	0.5442
X_2X_4	0.226	0.6441	1.120	0.3146	0.269	0.6151	0.262	0.6193
X_2X_5	0.809	0.3896	0.088	0.7726	0.026	0.8751	1.094	0.3201
X_3X_4	1.87	0.2019	2.194	0.1693	1.450	0.2562	2.167	0.1717
X_3X_5	1.76E-05	0.9967	0.505	0.4934	0.258	0.6219	0.013	0.9102
X_4X_5	31.8	0.0002[a]	32.7864	0.0002[a]	28.078	0.0003[a]	33.414	0.0002[a]

[a] Indicates the significant term

Figure 7a–d display the normal probability plot of the residuals for each response, Y_1, Y_2, Y_3, and Y_4. Notice that the residuals generally fall on a straight line, which implies that the errors are normally distributed. Furthermore, it adequately supports the least-squares fit. The results of comparison prove that the predicted values of Y_1, Y_2, Y_3, and Y_4 are close to those readings recorded in the experiment with a 95% confidence interval.

4.3 The effect of machining parameters on the vibration amplitudes

In the end-milling process, the machining parameters adopting the spindle speed (*N*), the feed rate (*f*), and the depth of cut (α_P) were chosen as the three numerical factors so as to investigate the influences on the vibration amplitude. The influences of machining parameters on the performance of the vibration amplitude have been analyzed, which is based on the above-proposed mathematical model in Section 4.2.

Figure 8 shows the response surface and contour plot for the *X*-axial, *Y*-axial, and *Z*-axial vibration amplitudes in relation to the spindle speed (*N*) and feed rate (*f*) with the cutting depth (α_P) maintained at the middle levels under the *X*-axial cutting feed direction and A-type tool holder. From Fig. 8, it can be seen that the tendency of the *X*-axial, *Y*-axial, and *Z*-axial vibration amplitudes slightly decreases with an increase of spindle speed. This event shows that the dynamic stiffness of MFTW system keeps constant during the end-milling process. Increasing the spindle speed promotes the rotation stability of spindle head, which results in suppressing the vibration amplitude. As seen above, the *X*-axial, *Y*-axial, and *Z*-axial vibration amplitudes obviously increase with increasing the feed rate. In the micro-cutting process, the vibration stability of cutting tool affects the quality of the machined surface. The status of feed rate corresponds to the amount of resistance force acting on the edge of cutting tool. This resistance force for the workpiece is regarded as the cutting force. The increase in the feed rate causes the increase of the resistance force in the cutting feed direction. Further increase in the feed rate causes the excited vibration appearance to appear more discontinuous chip.

In the cutting process, the resistance force acting on the cutting tool is mainly generated by the status of feed rate and depth of cut. The increase of cutting depth causes the increase in the resistance force at the tooltip, which excites more vibration appearance. The effects of feed rate (*f*) and depth of cut (α_P) on the *X*-axial, *Y*-axial, and *Z*-axial vibration amplitudes with keeping the spindle speed (*N*) at the middle levels under *X*-axial cutting feed direction and A-type tool holder are presented in Fig. 9. From Fig. 9, it can be obviously seen that the *X*-axial, *Y*-axial, and *Z*-axial vibration amplitudes increase with increasing the value of

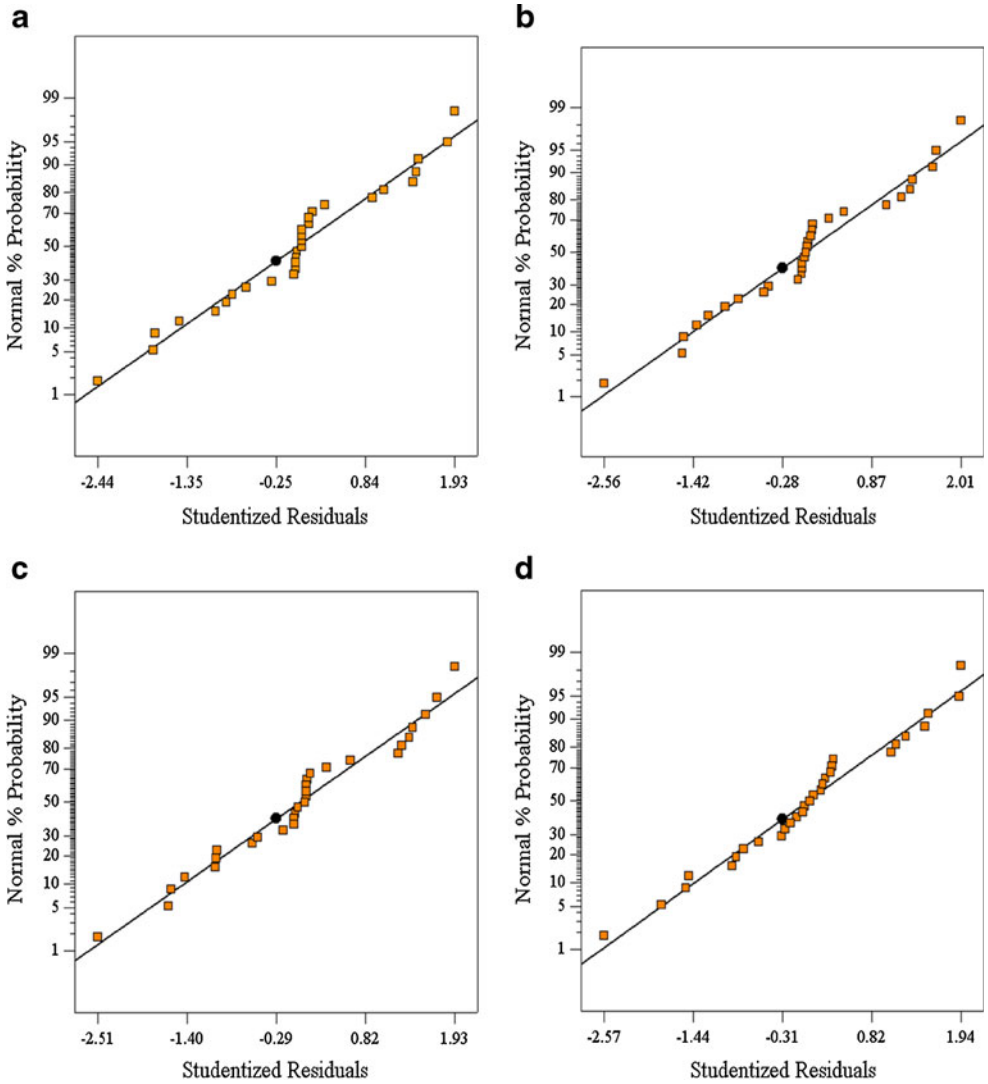

Fig. 7 Normal probability plot of residuals for each response: **a** surface roughness (Y_1), **b** *X*-axial vibration amplitude (Y_2), **c** *Y*-axial vibration amplitude (Y_3), and **d** *Z*-axial vibration amplitude (Y_4)

cutting depth. In general, the increase of cutting depth improves the resistance force, especially in the cutting feed direction.

According to the visualized time domain vibration data obtained from the experiments for various cutting conditions in Table 3, it is found that the average overall values of *Y*-axial and *Z*-axial vibration amplitudes have been enlarged by 4.71% and 69.28%, respectively, as compared with those of the *X*-axial vibration amplitude. As the results of analysis discussed above, the all vibration amplitudes are principally influenced by both the feed rate and cutting depth.

4.4 The effects of cutting feed direction and tool holder type

The status of cutting feed direction and tool holder type were regarded as the categorical factors in this study. The cutting feed direction represents the moving direction of spindle to provide the cutting action. During the end-milling process, the cutting tool edge removes material and meantime moves along the feed direction. As a result, the resistance force acting on the cutting tool derives from removing material and moving along feed direction. Therefore, the excited vibration amplitudes along the cutting feed direction are larger than those along other direction. Figure 10a and b reveal the vibration amplitudes in the *X*-axial, *Y*-axial, and *Z*-axial direction of the cutting tool under the *X*-axial and *Y*-axial cutting feed directions, respectively. It shows that the amplitude of vibration signals along the cutting feed direction is generally larger than that along other direction. But, from Fig. 10a, b, it can be seen that the tendency of the *Z*-axial vibration amplitudes are not obviously influenced by the cutting feed direction. This event is to identify the dynamic stiffness of spindle system along the *Z*-axial direction. As the cutting feed direction is along the *X*-axle, the average overall values of *X*-axial vibration amplitudes have increased by 5.08%, as compared with those of the *Y*-axial vibration amplitude according

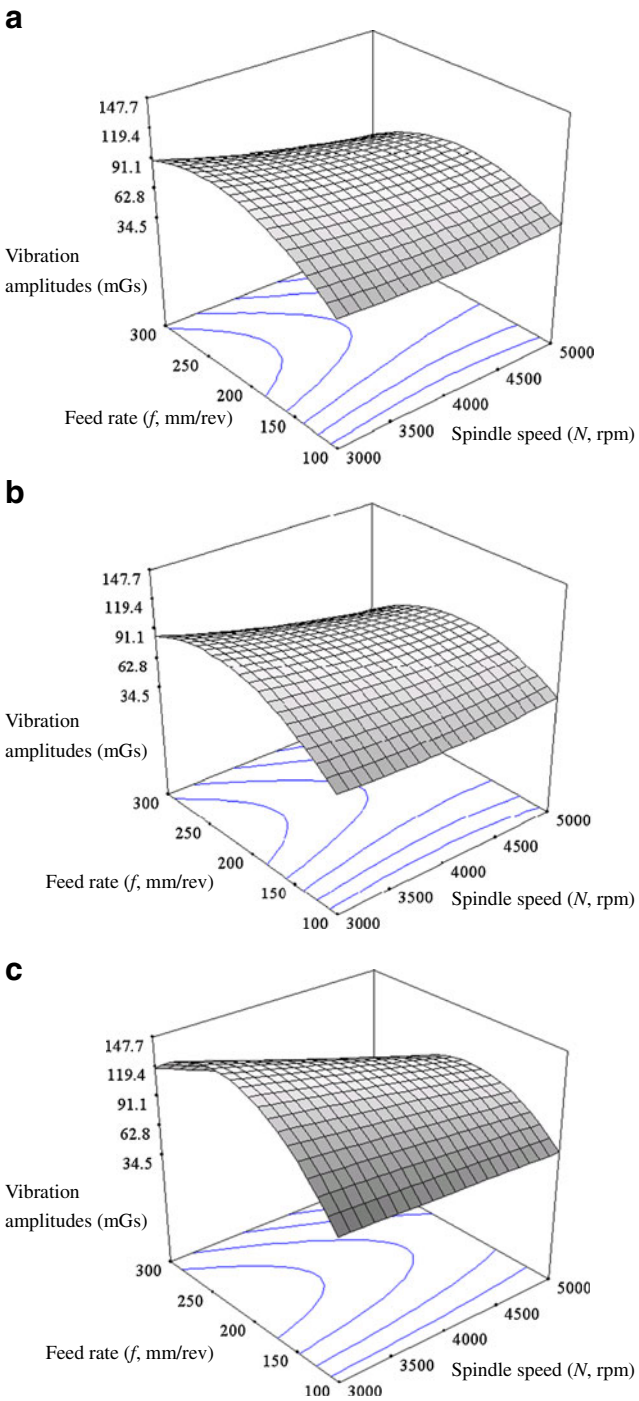

Fig. 8 The response surface and contour plot for the **a** *X*-axial, **b** *Y*-axial, and **c** *Z*-axial vibration amplitudes between the effect of spindle speed (*N*) and feed rate (*f*) with the cutting depth (α_P) maintained at the middle levels under the *X*-axial cutting feed direction and A-type tool holder

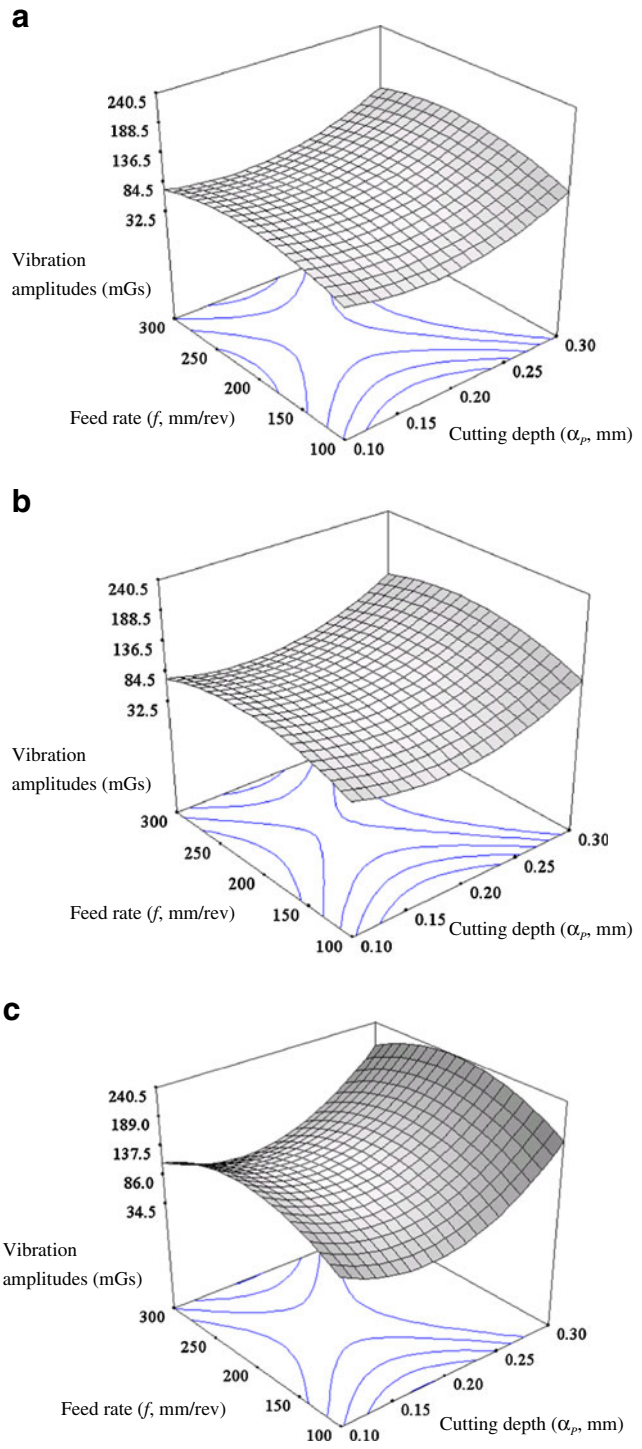

Fig. 9 The response surface and contour plot for the **a** *X*-axial, **b** *Y*-axial, and **c** *Z*-axial vibration amplitudes between the effect of feed rate (*f*) and cutting depth (α_P) with the spindle speed (*N*) maintained at the middle levels under the *X*-axial cutting feed direction and A-type tool holder

to the experimental data in Table 3. Simultaneously, the average overall values of *X*-axial vibration amplitudes under the *Y*-axial cutting feed direction have increased by 4.21%, as compared with those of the *Y*-axial vibration amplitude. The effect of cutting feed direction on the *X*-axial and *Y*-axial vibration amplitudes is identical in the whole variation capacity.

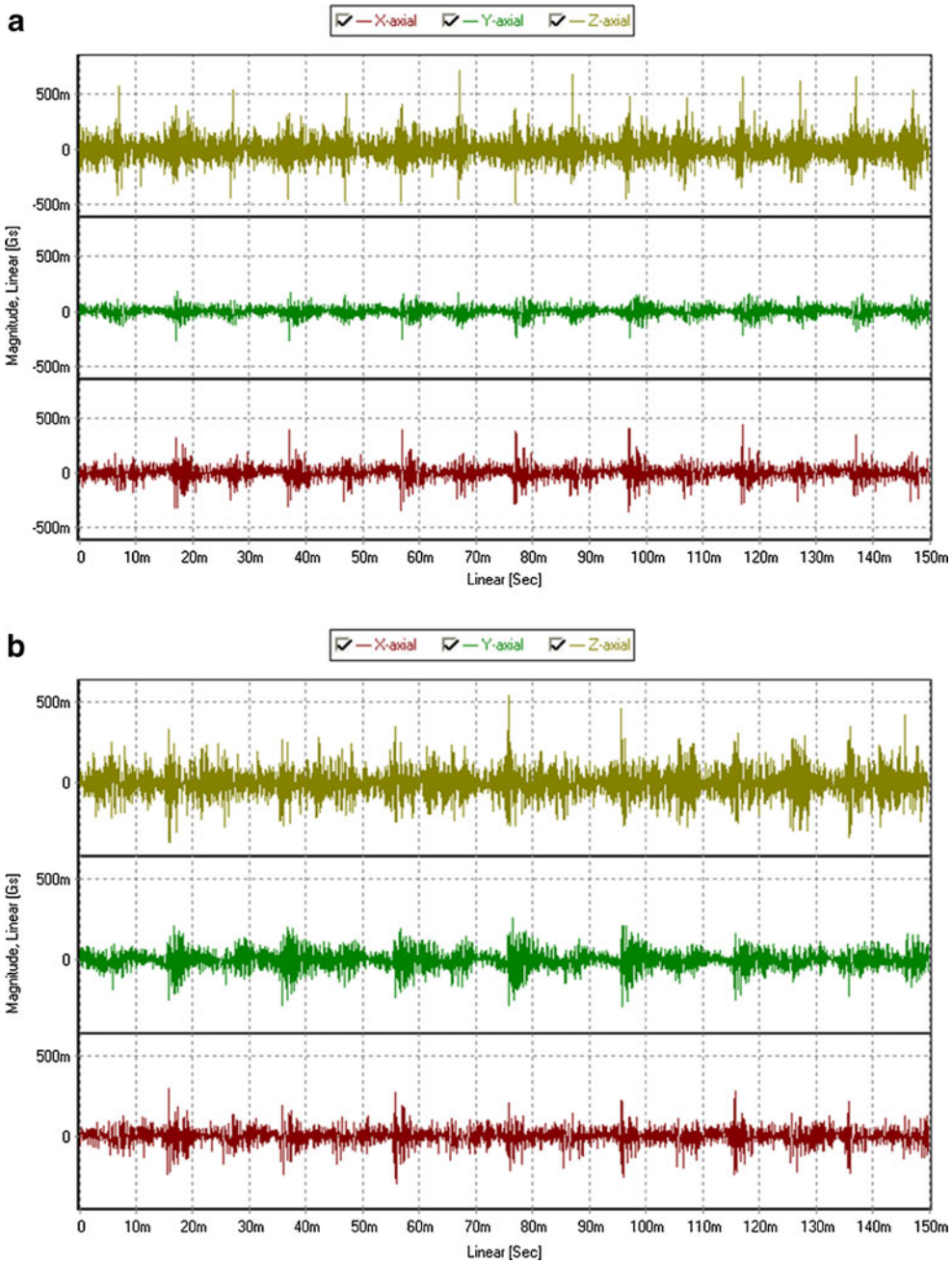

Fig. 10 The vibration amplitudes in the *X*-axial, *Y*-axial, and *Z*-axial direction of the cutting tool under the **a** *X*-axial and **b** *Y*-axial cutting feed directions. (N=4,000 rppm, f=200 mm/rve, α_P=0.20 mm and A-type tool holder)

In the end-milling process, the cutting edge of tool insert runs through the length of the cutting portion as well as on the face radially up to a certain cutting depth. The amount of tool inserts for the tool holder is to provide the status of cutting point on the workpiece. The quantity of cutting point determines the non-steady-state cyclic conditions of the cutting process. Here, A type and B type of tool holder adopted in the experiment have two and three tool inserts, and present two and three cutting points in a period, respectively. Figure 11a, b reveal the vibration amplitudes in the *X*-axial, *Y*-axial, and *Z*-axial direction of the cutting tool using the A type and B type of tool holder, respectively. It is observed that the amplitude of vibration signals using the B type is generally smaller than that using the A type. The multi-point cutting process can be similar to the continuous cutting process, which represents a steady cyclic condition of cutting process. This event provides the more stability of overall vibration on the cutting tool, which leads to the results of the best machined surface and the continuous chip. According to the data in Table 3, it is found that the average overall values of *X*-axial, *Y*-axial, and *Z*-axial vibration amplitudes using B type tool holder have decreased by 12.2%, 14.71%, and 16.28%, respectively, as compared with those using A type tool hold.

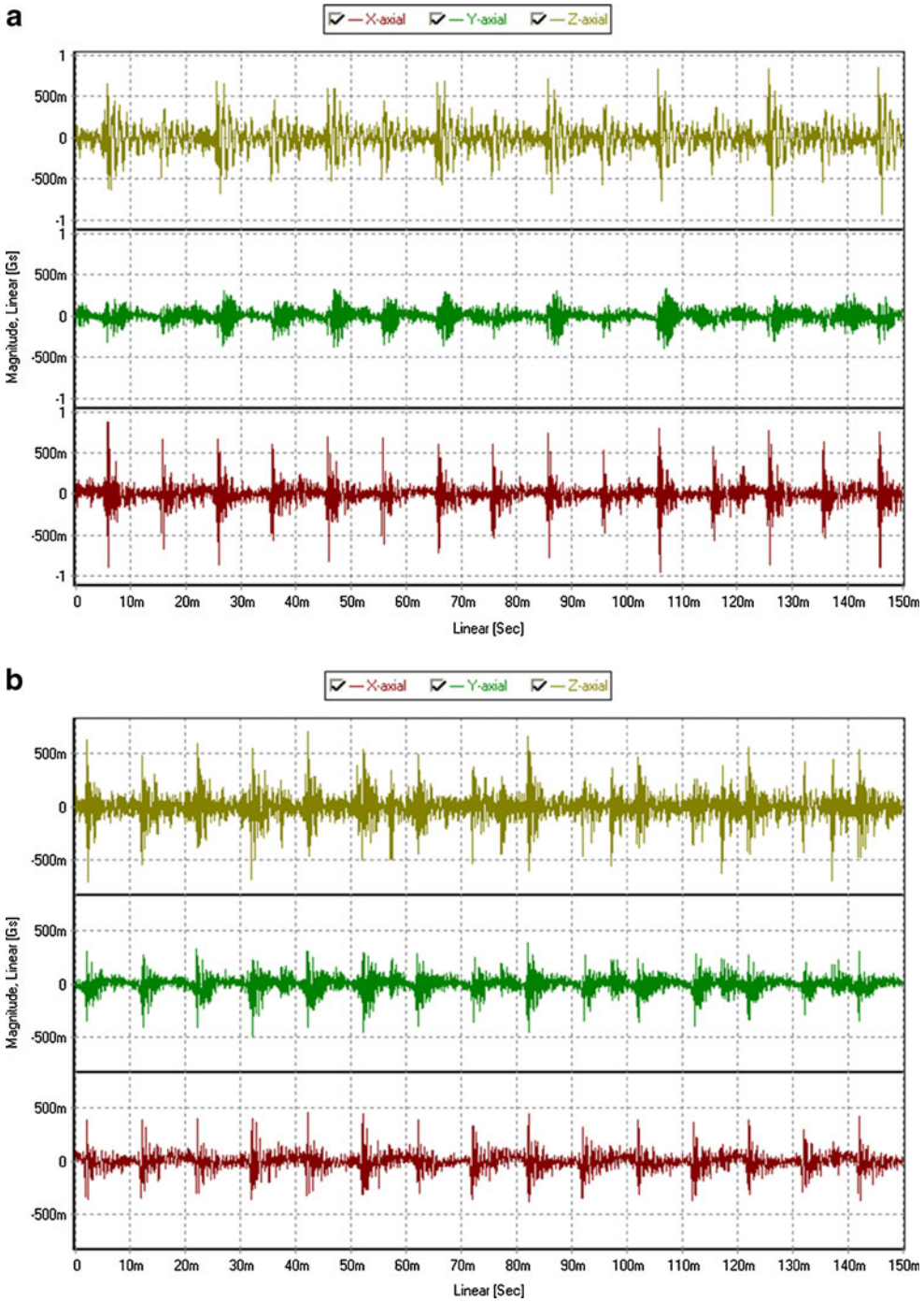

Fig. 11 The vibration amplitudes of the cutting tool using the **a** A type and **b** B type tool holder in the *X*-axial, *Y*-axial, and *Z*-axial direction, respectively

4.5 The machinability evaluation of surface roughness

More stability of cutting tool leads to the results of the best-machined surface and the continuous chip. Figure 12a–c displays the relation between the surface roughness and the vibration amplitude in the status of various spindle speed, feed rate, and cutting depth, respectively. The effect of spindle speed on the value of surface roughness is presented in Fig. 12a, which shows that the change of surface roughness is identical to the results of vibration amplitude in the Fig. 8. It displays that the surface roughness tends to decrease with the increase in the spindle speed. From Fig. 12b, it displays the relation between the surface roughness and the vibration amplitude in the status of various feed rate, which can prove that the effect of feed rate improves all the values of the surface roughness and the vibration amplitude. The effect of feed rate promotes the unstability of the overall vibration to cause the unstability of cutting process, and exhibits the result of the

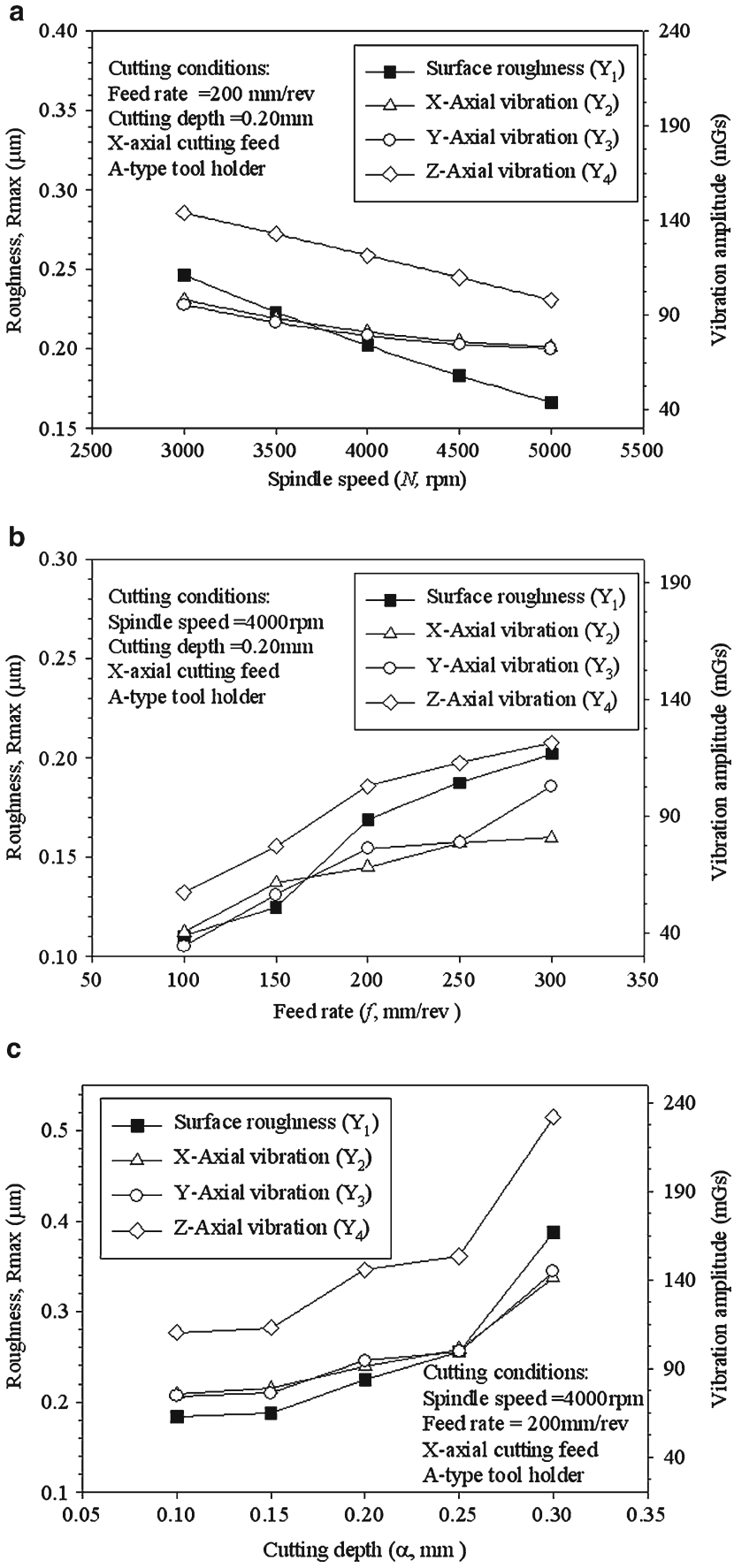

Fig. 12 The relation between the surface roughness and the vibration amplitude in the status of various parameters: **a** spindle speed, **b** feed rate, and **c** cutting depth

worst machined surface. Figure 12c displays the relation between the surface roughness and the vibration amplitude in the status of various cutting depth, and the cutting depth has obviously affected the surface roughness and the vibration amplitude. Consequently, the overall vibration in the tip of cutting tool is unfavorable to the roughness of the machined surface. Therefore, the best surface roughness is achieved at the highest spindle speed and lowest both feed rate and cutting depth as expected. These results had been attributed to the increase in spindle speed and decrease in both feed rate and cutting depth, which leads to the decrease in the cutting force and promotes the equivalent stiffness and damping coefficient of cutting tool tip, hence the machined surface has lower value of surface roughness.

Figure 13a, b displays the relation between the surface roughness and the vibration amplitude in the status of cutting feed direction and tool holder type, respectively. From the results of Section 4.4, the amplitude of vibration signals along the cutting feed direction is generally larger than that along other direction and hence the machined surface exhibits a worse quality in the cutting feed direction. But, the tendency of the *Z*-axial vibration amplitudes is not obviously by the cutting feed direction. The *Z*-axial vibration amplitudes play a dominant factor affecting the surface roughness. The effect of cutting feed direction on the overall vibration of cutting tooltip is not obvious, and hence, the variation of surface roughness identifies along any cutting feed direction. From Fig. 13b, it is observed that the machined surface using B-type tool holder presents a good quality. The overall vibration using B-type tool holder is more stable than that using A-type tool holder during the cutting process. The surface roughness of the machined surface using B-type

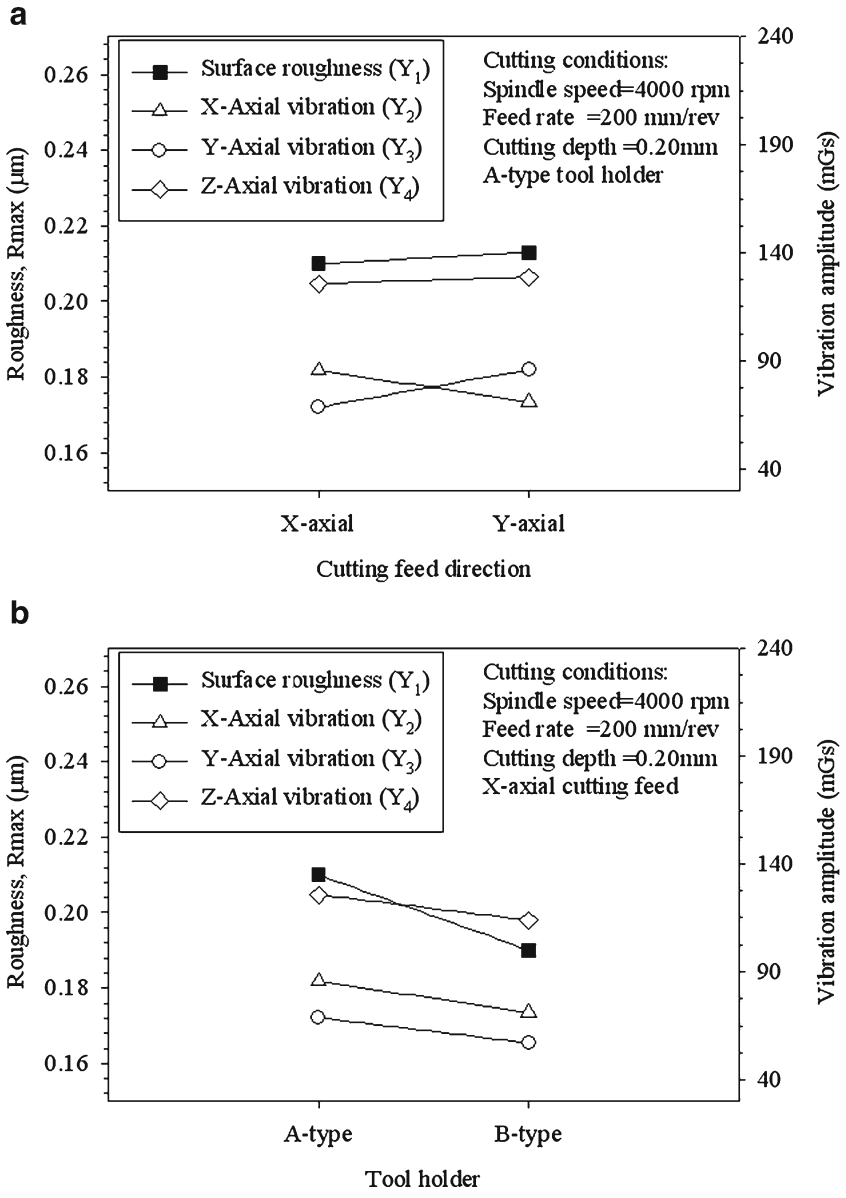

Fig. 13 The relation between the surface roughness and the vibration amplitude in the status of **a** cutting feed direction and **b** tool holder type

tool holder displays the reduction of 8.16%, compared to that using A-type tool holder in the same cutting conditions.

5 Conclusions

This research adopts the technology of SSA to extract and transform the raw signals of cutting tool vibrations for investigating the relationship between vibration and surface roughness in the precision end-milling process of hardened SCM440 steel. An experimental plan of a five-factor (three numerical plus two categorical) D-optimal design based on the RSM was employed to carry out the experimental study. According to the developed mathematical model, the machinability evaluation in the precision end-milling process has been analyzed and draws the following conclusions:

(1) The status of the vibration amplitudes between the cutting tooltip and workpiece is verified that the dominant factors will affect the surface roughness.
(2) The results of ANOVA confirm that the mathematical models of surface roughness and vibration amplitude obtained in this study are fairly well fitted with the experimental values with a 95% confidence interval.
(3) The effects of feed rate and cutting depth provide the reinforcement on the overall vibration to cause the unstability of cutting process and exhibit the result of the worst machined surface.
(4) Increasing the spindle speed promotes the rotation stability of spindle head, which results in suppressing the vibration amplitude. The amplitude of vibration signals along the cutting feed direction is generally larger than that along other direction.
(5) The cutting process using B-type tool holder (three inserts) is to benefit the stability of cutting tool, compared to that using A-type tool holder (two inserts) in the same cutting conditions. Hence, the machined surface exhibits a good quality.

References

1. Chae J, Park SS, Freiheit T (2006) Investigation of micro-cutting operations. Int J Mach Tools Manuf 46:313–332
2. Tounsi N, Otho A (2000) Identification of machine-tool–workpiece system dynamics. Int J Mach Tools Manuf 40:1367–1384
3. Cowley A (1970) Structural analysis. Machine tool structures. Pergamon, Oxford
4. Marinescu I, Ispas C, Boboc D (2002) Handbook of machine tool analysis. Marcel Dekker, New York
5. Dimla DE Sr (2004) The impact of cutting conditions on cutting forces and vibration signals in turning with plane face geometry inserts. J Mater Process Technol 155–156:1708–1715
6. Thomas M, Beauchamp Y, Youssef AY, Masounave J (1996) Effect of tool vibration on surface roughness during lathe dry turning process. Comput Ind Eng 31(3–4):637–644
7. Mer A, Diniz AE (1994) Correlating tool wear, tool life, surface roughness and tool vibration in finish turning with coated carbide tools. Wear 173:137–144
8. Jang DY, Choi YG, Kim HG, Hsiao A (1996) Study of the correlation between surface roughness and cutting vibration to develop an online roughness measuring technique in hard turning. Int J Mach Tools Manuf 36(4):453–464
9. Abouelatta OB, Madl J (2001) Surface roughness prediction based on cutting parameters and tool vibrations in turning operations. J Mater Process Technol 118:269–277
10. Dimla DE (2002) The correlation of vibration signal features to cutting tool wear in a metal turning operation. Int J Adv Manuf Technol 19:705–713
11. Risbood KA, Dixit US, Sahasrabudhe AD (2003) Prediction of surface roughness and dimensional deviation by measuring cutting forces and vibrations in turning. J Mater Process Technol 132(1–3):203–214
12. Li HZ, Zeng H, Chen XQ (2006) An experimental study of tool wear and cutting force variation in the end milling of Inconel 718 with coated carbide inserts. J Mater Process Technol 180:296–304
13. Golyandina N, Nekrutkin V, Zhigljavsky A (2001) Analysis of time series structure—SSA and related techniques. Chapman &Hall/CRC, Boca Raton, pp 13–17
14. Salgado DR, Alonso FJ (2006) Tool wear detection in turning operations using singular spectrum analysis. J Mater Process Technol 171:451–458
15. Kilundu B, Dehombreux P, Chiementin X (2011) Tool wear monitoring by machine learning techniques and singular spectrum analysis. Mech Syst Signal Process 25:400–415
16. Myers RH, Montgomery DC (1995) Response surface methodology: process and product optimization using designed experiments. John Wiley and Sons, New York
17. Khuri AI, Cornell JA (1996) Response surfaces, designs and analyses. Marcel Dekker, New York
18. Puri AB, Bhattacharyya B (2005) Modeling and analysis of white layer depth in a wire-cut EDM process through response surface methodology. Int J Adv Manuf Technol 25:301–307
19. Lin BT, Jean MD, Chou JH (2007) Using response surface methodology with response transformation in optimizing plasma spraying coatings. Int J Adv Manuf Technol 34:307–315
20. Davim JP, Gaitonde VN, Karnik SR (2008) An investigative study of delamination in drilling of medium density fibreboard (MDF) using response surface models. Int J Adv Manuf Technol 37:49–57
21. Palanikumar K (2008) Application of Taguchi and response surface methodologies for surface roughness in machining glass fiber reinforced plastics by PCD tooling. Int J Adv Manuf Technol 36:19–27
22. Çaydaş U, Hasçalik A (2008) Modeling and analysis of electrode wear and white layer thickness in die-sinking EDM process through response surface methodology. Int J Adv Manuf Technol 38:1148–1156
23. Munda J, Bhattacharyya B (2008) Investigation into electrochemical micromachining (EMM) through response surface methodology based approach. Int J Adv Manuf Technol 35:821–832
24. Box GEP, Lucas HL (1959) Design of experiments in non-linear situations. Biometrika 46(1/2):77–90